

## MINERALOGICAL TRANSFORMATIONS IN SERPENTINITES FROM THE MT. CAPANNE THERMOMETAMORPHIC AUREOLE (ELBA ISLAND, ITALY)

MARCO FERRARI

Dipartimento di Scienze della Terra, Università degli Studi di Siena, Via Laterina 8, 53100 Siena

### INTRODUCTION

Following the collisional phase of the early Miocene, which led to the basic structure of the Apennines, Elba Island was affected by extensional tectonics related to the opening of the Tyrrhenian Sea and by the emplacement of the monzogranitic pluton of Mount Capanne 6.9 Ma ago with three pulses of magma (Dini *et al.*, 2002; Farina *et al.*, 2010). The monzogranitic intrusion caused the contact metamorphism and the formation of a clear thermometamorphic aureole that involved ultramafic rocks.

In eastern and central Elba Island, massive serpentinites consist of typical retrograde pseudomorphic textures, *i.e.* mesh rims/cores and bastites, resulting from olivine and pyroxene serpentinization, respectively. Mesh rims, representing early hydration, are formed by isoriented sectors of crystalline 1T lizardite, whereas bastites and mesh cores, corresponding to late fast serpentinization, are formed by poorly crystalline assemblages of tiny lizardite lamellae, chrysotile, and polygonal serpentine fibers, in random orientation (Viti & Mellini, 1998). Relics of peridotitic olivine and pyroxene are rare, indicating advanced serpentinization (Rumori *et al.*, 2004; Viti *et al.*, 2005). On the contrary, the thermometamorphic serpentinites of the aureole of Mt. Capanne show rare traces of pseudomorphic textures with preserved serpentine; they are abundantly composed by talc, chlorite, anthophyllite, tremolite and olivine (thermometamorphic minerals).

This research is aimed at characterizing the mineralogical and micro/nanostructural transformations, as well as the reaction mechanisms (both prograde and retrograde) of the serpentinites from the thermometamorphic aureole of Mt. Capanne. Fourteen samples were collected, on which the following whole-rock analyses were made by means of X-ray fluorescence (XRF), X-ray powder diffraction (XRPD), LOI - and  $\text{Fe}^{2+}/\text{Fe}^{3+}$  - determination, together with a petrographic study using optical microscopy. The results provided a complete chemical and mineralogical characterization of the individual samples, as well as a prior information about the metamorphic grade. Finally, a SEM/EDS study and, more widely, a TEM/EDS study were undertaken on particular sites deemed to be significant, in order to better understand and describe the individual reactions.

### PRINCIPAL PROGRADE REACTIONS

The results of this study have highlighted four main prograde reactions and two retrograde reactions.

The first prograde reaction takes place both in bastites and mesh cores and leads to the formation of antigorite. Antigorite grows in the form of lamellae, longer than 50  $\mu\text{m}$ , with random orientation; it develops at the expense of low-crystallinity serpentine, with a growth process that occurs predominantly, in the direction of the elongation, by amorphization of the pre-existing phase and recrystallization of the new phase. The individual antigorite lamellae join each other along their direction of elongation during their growth, thus originating sutures inside the more developed lamellae. The TEM/EDS study has permitted to understand that antigorite has a highly defective structure since modulation, dislocation and polysynthetic twinning occur (Fig. 1).

The second prograde reaction leads to a fine intergrowth of talc and chlorite starting from the low-crystallinity serpentine of the bastites. TEM images suggest that talc within bastites grows in the form of very long and rather thin lamellae (typical thickness of 30 - 60 nm), which are finely intercalated to low-crystallinity serpentine characterized by high porosity (Fig. 2). Talc is always associated with lesser amount of chlorite. The lamellae of chlorite show a rather variable width, but they are always wider than the talc lamellae. Portions of poorly crystalline serpentine are very often present within the lamellae of chlorite. High-resolution images and

SAED patterns showed that also chlorite is often affected by structural defects, generally concentrated in specific crystal portions rather than homogeneously distributed (Fig. 3).

The third prograde reaction causes the formation of anthophyllite and/or tremolite amphiboles. Prograde amphiboles can nucleate both in bastites and mesh textures (Fig. 4). Within bastite, they may grow as tiny

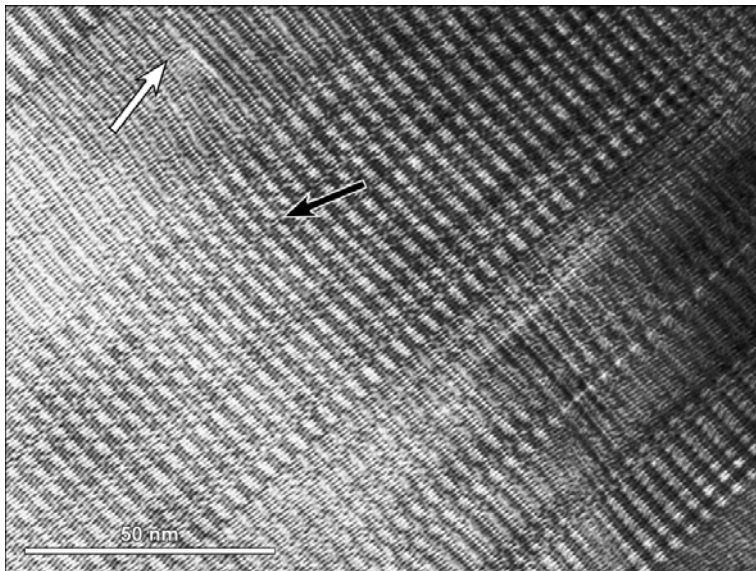


Fig. 1 - Antigorite with polysynthetic twinning (e.g. black arrow) and modulation dislocation (white arrow).

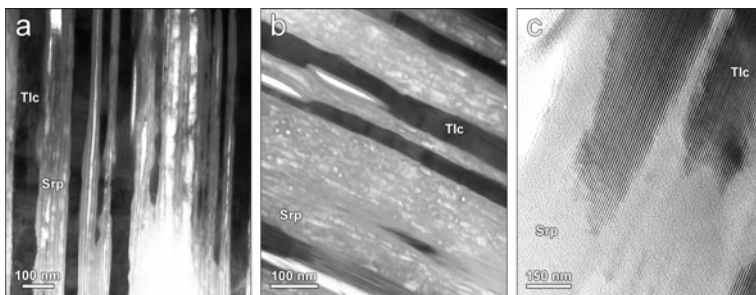


Fig. 2 - (a) Low magnification TEM image of a bastite where iso-oriented and elongated lamellae of talc are intergrown with a poorly crystalline serpentine. (b) Talc lamellae within a bastite; few recognizable traces of chrysotile fibres and elongated lacerations are present within the poorly crystalline serpentine. (c) Detail of talc lamellae terminations in a serpentine bastite. The talc lamellae show a rather irregular shape.

acicular crystals with size around 100  $\mu\text{m}$  in length, developing in random orientation, without evident microstructural control by the pre-existing bastite, and evolving to a fine-grained interpenetrating felt. Alternatively, they may progressively replace the bastitic serpentine from the outer toward the inner portions, producing a large pseudomorphic single crystal, after the original bastitic lamella. In mesh textures, amphiboles typically occur as elongated crystals, up to millimeter sizes, with an acicular-fibrous habit. Their orientation is completely independent from the pre-existing pseudomorphic texture. At their terminations, acicular amphiboles typically separate into sub-fibres. In some cases anthophyllite and tremolite coexist within meshes where they show a fibrous habit. High-resolution TEM images and SAED patterns showed that anthophyllite is crystalline and homogeneous; moreover, although the structure can be locally ordered, there are often evidences of polytypic disorder attributed to the simultaneous presence of different polytypes. In fact, SAED data indicate a complex association of orthorhombic (both *Pnmm* protoanthophyllite and *Pnma* anthophyllite) and monoclinic *C2/m* polytypes (cumingtonite). The occurrence of protoanthophyllite within this kind of rocks is in agreement with previous findings; in

fact, protoanthophyllite (as well as the proto-polymorphs of jimthompsonite and chesterite) has been already detected within ultramafic rocks that have experienced thermal metamorphism (Konishi *et al.*, 2002, 2003, 2008), or in pegmatites (Sueno *et al.*, 1998), thus pointing to a high-T, low-P stability field relative to magnesian amphibole. The anthophyllite also shows evident retrograde processes which determine the formation of

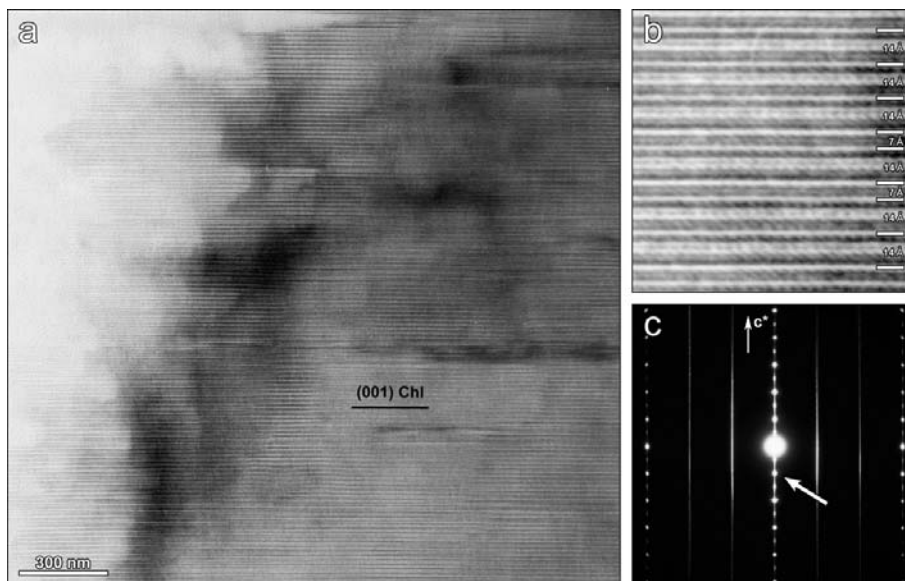


Fig. 3 - (a) TEM image of a chlorite lamella with stacking disorder along [001]. (b) HRTEM image of chlorite. Packets of 14 Å and packets of 7 Å alternate disorderly along *c* axis. (c) Chlorite *b\** *c\** SAED pattern with intense streaking along *c\**. The typical 14 Å reflections of chlorite are sharp and intense (arrow) whereas the 7 Å reflections are more diffuse and elongated.

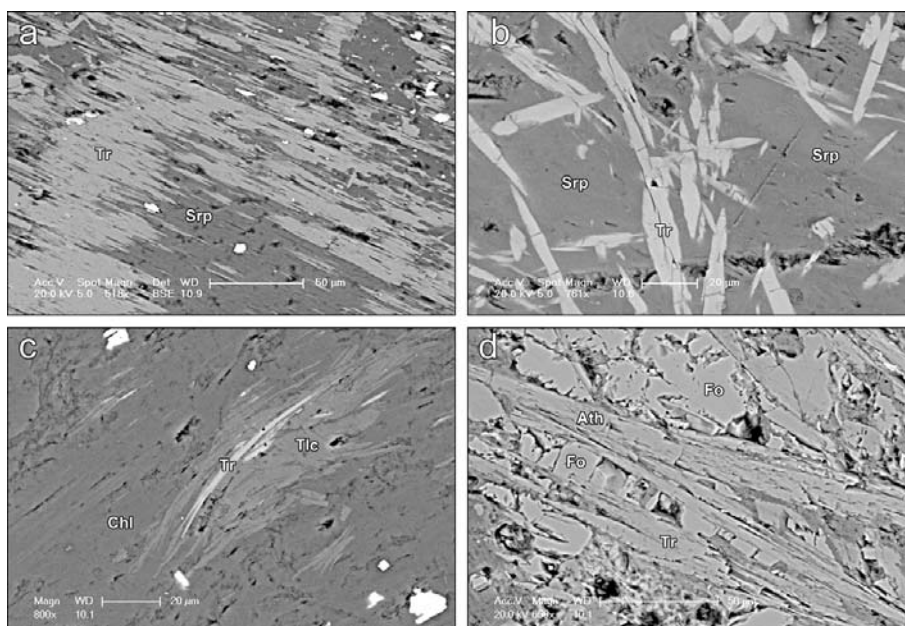


Fig. 4 - (a) SEM/BSE image representative of a bastite partly replaced by tremolite; tremolite crystals tend to grow from the outer edges to the centre of the bastite. (b) SEM/BSE image representative of a bastite with acicular crystals of tremolite growing with no textural relationships with the bastite itself. (c) SEM/BSE image showing a bastite with tremolite acicular crystals at the beginning of their formation. (d) SEM/BSE image of a forsterite recrystallized mesh area with amphibole crystals growing with a fibrous habit.

serpentine and, more rarely, of talc. On the other hand, the TEM/EDS analyses, performed on tremolite within bastites and meshes, indicate that it is very ordered and not affected by particular retrograde processes.

The fourth prograde reaction observed in the examined samples leads to the formation of forsteritic olivine, which replaces serpentine on meshes. Both the optical microscopy and SEM observations showed that

forsteritic olivine, which replaces serpentine on meshes. Both the optical microscopy and SEM observations showed that forsterite produces extremely variable textures attributable to five main cases (Fig. 5):

1) Single forsterite crystals that replace the entire core of the meshes: adjacent cores do not have common optical orientation (textures 1a and 1b in Fig. 5);

2) Single forsterite crystals that replace the entire core of the meshes: adjacent cores show common optical orientation (textures 2a and 2b in Fig. 5);

3) Single forsterite crystals that replace the entire core of the meshes (generally, with relations of optical continuity between adjacent cores): mesh rims are replaced by microgranular forsterite finely associated with the original serpentine (texture 3 in Fig. 5);

4) Associations of micro-crystalline forsterite (more or less isoriented), which, unlike the cases from 1 to 3, does not show any relationship with previous pseudomorphic textures (texture 4 in Fig. 5);

5) Portions formed by forsterite crystals in close contact each other, or with a thin layer of microgranular olivine at the grain boundaries. The adjacent crystals have generally a random orientation (texture 5 in Fig. 5).

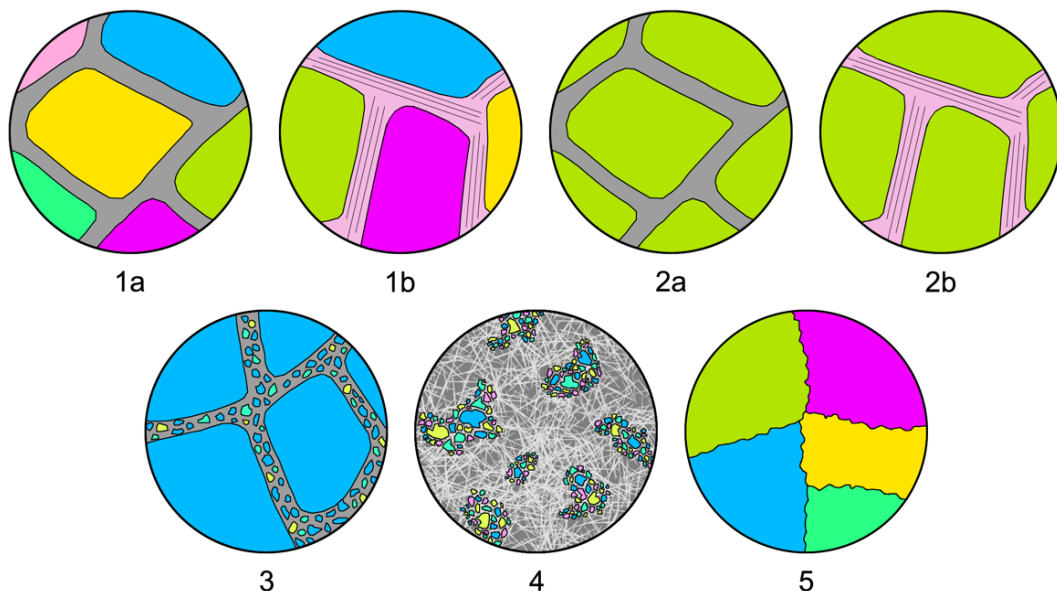


Fig. 5 - Schematic representation of the main typical forsterite textures in the thermometamorphic serpentinites of the Mt. Capanne. The different colours correspond to different values of birefringence. The grey material in textures 1a, 2a and 3 corresponds to serpentine, whereas the pink laminated material in textures 1b and 2b corresponds to prograde phyllosilicates (mainly talc).

In addition to the complete characterization of textures produced by forsterite, these observations allow to affirm that forsterite nucleation occurs only within mesh textures, and never in bastites, even when the mesh texture is replaced by a prograde texture with interpenetrating antigorite.

Finally, these observations evidenced a clear crystallization sequence which determines the serpentine replacement from the core to the rim.

In any case, TEM observations on thermometamorphic olivines suggest that the serpentine-forsterite transformation takes place through an amorphization and a subsequent recrystallization process, both when forsterite replaces retrograde serpentine and when it replaces other prograde phyllosilicates (such as talc, chlorite, and antigorite).

The formation of forsterite single crystals inside the cores and the formation of millimeter-sized forsterite “macrocrystals” (due to adjacent cores isorientation) is probably the most difficult feature to explain. However,

the present study attempts to give an explanation considering all the possible cases of structural control related to the pre-existing textures and mineralogy.

## RETROGRADE REACTIONS

In addition to the prograde reactions described above, this study revealed the presence of two main retrograde reactions: the first is related to the anthophyllite retrograde processes, whereas the second leads to the olivine alteration.

The most important retrograde reaction is certainly the one that leads to the serpentinization of magnesian amphibole. This process occurs on amphiboles that grow either in bastites or in mesh textures. The optical microscopy and the SEM/EDS analyses reveal that sub-parallel veins of serpentine cut Mg amphibole crystals; these are the main sites where the amphibole breakdown reaction starts. At the TEM scale, these fractures, or at least the cleavage planes, represent the starting surfaces for biopyriboles chains, which can be considered the first hydration product. High-resolution observations show that biopyriboles never cut the fracture surfaces, occur in disordered sequence, and have different chain widths. The TEM/EDS investigation, performed on Mg amphibole affected by retrograde processes, revealed the presence of several serpentine veins (Fig. 6). Many serpentine inclusions are also present close to the veins; they often have an elongated shape and are certainly subsequent to the biopyribole chains. In some cases, crystal portions affected by an advanced hydration stage and entire sectors totally replaced by serpentine were observed.

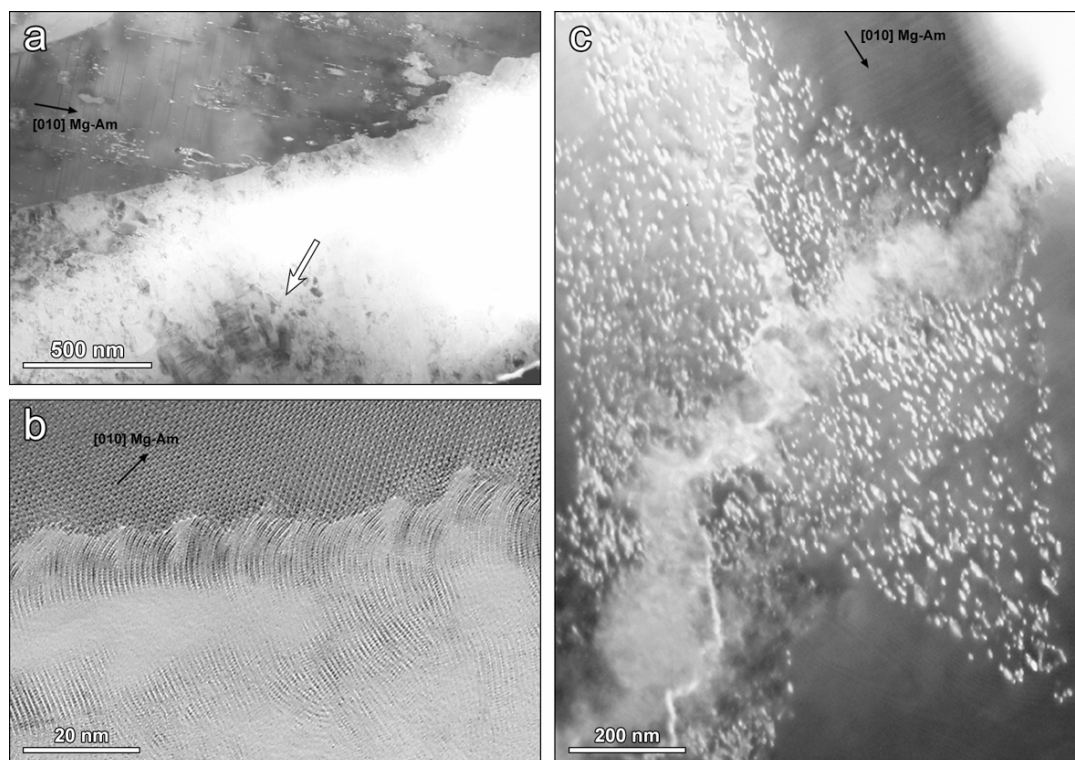


Fig. 6 - (a) TEM image of a wide serpentine vein (bright area) cutting defective Mg amphibole (dark area); the vein is predominantly filled by chrysotile and poorly crystalline serpentine, together with minor lizardite sectors (arrow). (b) HR detail of the interface between reacting amphibole and vein serpentine; at the reaction front, serpentine is almost always characterized by layer curling. (c) Magnesian amphibole crystal (dark area), cut by two intersecting serpentine veins (bright bands), characterized by irregular boundaries, approximately parallel to  $(010)_{\text{Mg-Am}}$  and  $(210)_{\text{Mg-Am}}$  (central and upper veins, respectively). Magnesian amphibole hosts many tiny serpentine inclusions (bright "spots"), whose distribution is clearly controlled by the host crystal structure.

Finally, the olivine alteration was also characterized; at the scale of optical microscopy it is recognizable by the clear brown to red colour in plane-polarized light. The TEM/EDS investigation suggested that the material has a low crystallinity like that of iddingsite.

#### REFERENCES

- Dini, A., Innocenti, F., Rocchi, S., Tonarini, S., Westerman, D.S. (2002): The magmatic evolution of the late Miocene laccolith-pluton-dyke granitic complex of Elba Island, Italy. *Geol. Mag.*, **139**, 257-279.
- Farina, F., Dini, A., Innocenti, F., Rocchi, S., Westerman, S. (2010): Rapid incremental assembly of the Monte Capanne pluton (Elba Island, Tuscany) by downward stacking of magma sheets. *Geol. Soc. Am. Bull.*, **122**, 1463-1479.
- Konishi, H., Dódoni, I., Buseck, P.R. (2002): Protoanthophyllite from three metamorphosed serpentinites. *Am. Mineral.*, **87**, 1096-1103.
- Konishi, H., Groy, T.L., Dódoni, I., Miyawaki, R., Matsubara, S., Buseck, P.R. (2003): Crystal structure of protoanthophyllite: A new mineral from the Takase ultramafic complex, Japan. *Am. Mineral.*, **88**, 1718-1723.
- Konishi, H., Buseck, P.R., Xu, H., Li, X. (2008): Proto-polymorphs of jimthompsonite and chesterite in contact-metamorphosed serpentinites from Japan. *Am. Mineral.*, **93**, 351-359.
- Rumori, C., Mellini, M., Viti, C. (2004): Oriented, non-topotactic olivine → serpentine replacement in mesh-textured, serpentinized peridotites. *Eur. J. Mineral.*, **16**, 731-741.
- Sueno, S., Matsuura, S., Gibbs, G.V., Boisen, M.B., Jr. (1998): A crystal chemical study of protoanthophyllite: orthoamphiboles with the protoamphibole structure. *Phys. Chem. Minerals*, **25**, 366-377.
- Viti, C. & Mellini, M. (1998): Mesh textures and bastites in the Elba retrograde serpentinites. *Eur. J. Mineral.*, **10**, 1341-1359.
- Viti, C., Mellini, M., Rumori, C. (2005): Exsolution and hydration of pyroxene from partially serpentinized harzburgites. *Mineral. Mag.*, **69**, 491-507.